Check for updates

Received: 5 February 2024 | Revised: 14 June 2024 | Accepted: 19 June 2024

DOI: 10.1002/hbm.26776

RESEARCH ARTICLE

WILEY

Dynamic properties in functional connectivity changes and striatal dopamine deficiency in Parkinson's disease

Adrian L. Asendorf[1] | Hendrik Theis[1,2] | Marc Tittgemeyer[3,4] | Lars Timmermann[5] | Gereon R. Fink[2,6] | Alexander Drzezga[1] | Carsten Eggers[5,7] | Marina C. Ruppert-Junck[5] | David J. Pedrosa[8] | Merle C. Hoenig[1,9] | Thilo van Eimeren[1,2]

[1]Department of Nuclear Medicine, University of Cologne, Faculty of Medicine and University Hospital Cologne, Cologne, Germany

[2]Department of Neurology, University of Cologne, Faculty of Medicine and University Hospital Cologne, Cologne, Germany

[3]Max Planck Institute for Metabolism Research, Translational Neurocircuitry Group, Cologne, Germany

[4]University of Cologne, Cologne Excellence Cluster on Cellular Stress Responses in Aging-Associated Diseases (CECAD), Cologne, Germany

[5]Department of Neurology, Marburg, Germany

[6]Research Centre Juelich, Institute of Neuroscience and Medicine III, Cognitive Neuroscience, Juelich, Germany

[7]Department of Neurology, University of Duisburg-Essen, Knappschaftskrankenhaus Bottrop, Bottrop, Germany

[8]Universities of Marburg and Gießen, Center for Mind, Brain, and Behavior-CMBB, Marburg, Germany

[9]Research Center Juelich, Institute of Neuroscience and Medicine II, Molecular Organization of the Brain, Juelich, Germany

Correspondence
Thilo van Eimeren, Department of Nuclear Medicine, University of Cologne, Faculty of Medicine and University Hospital Cologne, Cologne, Germany.
Email: thilo.van-eimeren@uk-koeln.de

Funding information
Deutsche Forschungsgemeinschaft (DFG, German Research Foundation), Grant/Award Numbers: 431549029, 413543196

Abstract

Recent studies in Parkinson's disease (PD) patients reported disruptions in dynamic functional connectivity (dFC, i.e., a characterization of spontaneous fluctuations in functional connectivity over time). Here, we assessed whether the integrity of striatal dopamine terminals directly modulates dFC metrics in two separate PD cohorts, indexing dopamine-related changes in large-scale brain network dynamics and its implications in clinical features. We pooled data from two disease-control cohorts reflecting early PD. From the Parkinson's Progression Marker Initiative (PPMI) cohort, resting-state functional magnetic resonance imaging (rsfMRI) and dopamine transporter (DaT) single-photon emission computed tomography (SPECT) were available for 63 PD patients and 16 age- and sex-matched healthy controls. From the clinical research group 219 (KFO) cohort, rsfMRI imaging was available for 52 PD patients and 17 age- and sex-matched healthy controls. A subset of 41 PD patients and 13 healthy control subjects additionally underwent ^{18}F-DOPA-positron emission tomography (PET) imaging. The striatal synthesis capacity of ^{18}F-DOPA PET and dopamine terminal quantity of DaT SPECT images were extracted for the putamen and the caudate. After rsfMRI pre-processing, an independent component analysis was performed on both cohorts simultaneously. Based on the derived components, an individual sliding window approach (44 s window) and a subsequent k-means

This is an open access article under the terms of the Creative Commons Attribution-NonCommercial License, which permits use, distribution and reproduction in any medium, provided the original work is properly cited and is not used for commercial purposes.
© 2024 The Author(s). *Human Brain Mapping* published by Wiley Periodicals LLC.

clustering were conducted separately for each cohort to derive dFC states (reemerging intra- and interindividual connectivity patterns). From these states, we derived temporal metrics, such as average dwell time per state, state attendance, and number of transitions and compared them between groups and cohorts. Further, we correlated these with the respective measures for local dopaminergic impairment and clinical severity. The cohorts did not differ regarding age and sex. Between cohorts, PD groups differed regarding disease duration, education, cognitive scores and L-dopa equivalent daily dose. In both cohorts, the dFC analysis resulted in three distinct states, varying in connectivity patterns and strength. In the PPMI cohort, PD patients showed a lower state attendance for the globally integrated (GI) state and a lower number of transitions than controls. Significantly, worse motor scores (Unified Parkinson's Disease Rating Scale Part III) and dopaminergic impairment in the putamen and the caudate were associated with low average dwell time in the GI state and a low total number of transitions. These results were not observed in the KFO cohort: No group differences in dFC measures or associations between dFC variables and dopamine synthesis capacity were observed. Notably, worse motor performance was associated with a low number of bidirectional transitions between the GI and the lesser connected (LC) state across the PD groups of both cohorts. Hence, in early PD, relative preservation of motor performance may be linked to a more dynamic engagement of an interconnected brain state. Specifically, those large-scale network dynamics seem to relate to striatal dopamine availability. Notably, most of these results were obtained only for one cohort, suggesting that dFC is impacted by certain cohort features like educational level, or disease severity. As we could not pinpoint these features with the data at hand, we suspect that other, in our case untracked, demographical features drive connectivity dynamics in PD.

Practitioner Points

- Exploring dopamine's role in brain network dynamics in two Parkinson's disease (PD) cohorts, we unraveled PD-specific changes in dynamic functional connectivity.
- Results in the Parkinson's Progression Marker Initiative (PPMI) and the KFO cohort suggest motor performance may be linked to a more dynamic engagement and disengagement of an interconnected brain state.
- Results only in the PPMI cohort suggest striatal dopamine availability influences large-scale network dynamics that are relevant in motor control.

KEYWORDS
DAT SPECT, dynamic functional connectivity, F-DOPA PET, imaging, network, resting-state fMRI

1 | INTRODUCTION

Parkinson's disease (PD) is characterized by a degeneration of the nigrostriatal dopaminergic neurons, causing a wide range of motor and non-motor symptoms. Region-specific associations have revealed a strong relationship between striatal dopamine availability, motor symptom severity (Asenbaum et al., 1997; Benamer et al., 2000; Pirker, 2003), and higher-order cognitive tasks (Cools, 2011; Costa et al., 2014). From a network-based perspective, this suggests dopamine is a crucial player in effectively recruiting large-scale networks associated with these cognitive and motor domains. Using resting-state functional magnetic resonance imaging (rsfMRI) to investigate connectivity across different networks has repeatedly shown that the putamen, which is known to express the most prominent striatal

10970193, 2024, 10, Downloaded from https://onlinelibrary.wiley.com/doi/10.1002/hbm.26776 by Bibl. der Universitat zu Koln, Wiley Online Library on [13/11/2026]. See the Terms and Conditions (https://onlinelibrary.wiley.com/terms-and-conditions) on Wiley Online Library for rules of use; OA articles are governed by the applicable Creative Commons License

dopamine reduction in clinical PD, loses connectivity strength with frontal brain structures (Rolinski et al., 2016). Further, in recent multimodal approaches incorporating dopamine positron emission tomography (PET) or dopamine transporter (DaT) single-photon emission computed tomography (SPECT), it has been illustrated that the degeneration of nigrostriatal connectivity functionally impairs distinct striatocortical (Ruppert et al., 2020) and putamen-midbrain (Rieckmann et al., 2015) projections.

Additionally, an increase in dopaminergic deficit was associated with decreased putaminal interconnectivity over time (Li et al., 2020). These studies suggest that dopamine is fundamental for the efficient interplay between motor processing areas and parts of the basal ganglia. Interestingly, PD-specific changes in large-scale network organization normalize after taking dopaminergic medication (P. T. Bell et al., 2015; Cole et al., 2013; Wu et al., 2009). Thus, network consequences of dopamine loss may not be limited to brain regions directly connected to the basal ganglia. However, how striatal dopamine deficiency specifically perturbs the interplay of large-scale brain networks remains unresolved.

Notably, most of these studies assessing network organization modulated by dopamine capacity in PD have typically assumed temporal stability and, hence, time-averaged functional networks across the resting-state data acquisition. However, functional networks dynamically fluctuate within scales of seconds and minutes (Chang & Glover, 2010). Incorporating the temporal features of spontaneous functional connectivity (FC) fluctuations in a dynamic FC analysis (dFC) aims to characterize these dynamics. How well the fluctuations in FC are aligned with actual brain dynamics is currently under debate. However, the note that dFC captures actual neural dynamics in the brain is supported by a growing body of literature (for review, see Lurie et al., 2020). Thus, dFC has been suggested to index changes in macroscopic neural activity patterns underlying critical aspects of cognition and behavior (Calhoun et al., 2014; Hutchison et al., 2013; Liégeois et al., 2019; Vidaurre et al., 2021). As dFC provides additional information about the temporal profile of brain function, it proposes the potential to improve our understanding of impaired brains and their changes in disorders. In fact, compared to the static approach, growing evidence suggests dFC to be a sensitive indicator for determining disability level (Tozlu et al., 2021) and distinguishing between individuals with pathological conditions and those without (Jin et al., 2017; Rashid et al., 2016). Concomitantly, altered network dynamics have been reported for various neuro-psychiatric conditions like schizophrenia (Damaraju et al., 2014; Fu et al., 2018; Sakoğlu et al., 2010; Yue et al., 2018), dementia (Córdova-Palomera et al., 2017; Jones et al., 2012; Schumacher et al., 2019), autism (de Lacy et al., 2017), major depression (Kaiser et al., 2015; Zhi et al., 2018), or epilepsy (Liu et al., 2017).

In PD, several recent whole-brain dFC accounts suggested the relevance of network dynamics in the clinical presentation of PD (Cao et al., 2023; Cordes et al., 2018; Díez-Cirarda et al., 2018; Fiorenzato et al., 2019; J. Kim et al., 2017). Importantly, these studies could show that PD-specific changes in dFC were linked to motor symptom severity (J. Kim et al., 2017), mild cognitive impairment (Díez-Cirarda et al., 2018; Fiorenzato et al., 2019), PD dementia (Fiorenzato et al., 2019), and autonomic dysfunction (Cao et al., 2023). Together, these studies emphasize that motor and cognitive impairments in PD appear to be driven by spatial *and* temporal alterations of large-scale network dynamics. However, reports concerning dFC in PD are inconsistent. While some studies suggested PD to be associated with a higher occurrence of highly interconnected states (i.e., reoccurring patterns of FC across time) (Díez-Cirarda et al., 2018; Kim et al., 2017), others demonstrated PD (Fiorenzato et al., 2019) and PD progression (Cao et al., 2023) to be associated with a higher occurrence of sparsely connected states. These inconsistent findings, however, may be due to methodological differences in data analyses and study design. Moreover, the currently available studies employing dFC in PD are limited to correlations with behavior or clinical severity and do not use quantified information about the degree of dopaminergic terminal loss. Direct investigations of the modulatory role of dopamine on dynamic network fluctuations are currently missing.

To this end, we analyzed datasets of two age- and sex-matched cohorts. The Parkinson's Progression Marker Initiative (PPMI) data set (https://www.ppmi-info.org/study-design/study-cohorts) included rsfMRI for 63 PD patients and 16 controls and DaT-SPECT as a measure for presynaptic dopaminergic dysfunction. In comparison, the KFO dataset (https://gepris.dfg.de/gepris/projekt/101434521?language=en) comprised 52 PD patients and 17 controls, including ^{18}F-Dopa PET as the measure of presynaptic dopaminergic impairment. The objectives of our study were as follows: First, to probe the reproducibility of our dFC analysis in two different PD cohorts. Second, to investigate the relationship between dopamine deficiency and large-scale network dynamics. To achieve this, we obtained PD-specific dFC changes by comparing the dFC variables of a healthy control group with a PD group for each cohort separately. Consequently, we tested whether these PD-specific dFC changes were associated with clinical cognition, motor scores, and dopamine availability in the striatum. We suspected PD-specific changes in dFC to appear in both groups. According to the literature discussed above, we expected these to be associated with either motor or cognitive function and dopaminergic deficit in the striatum.

2 | MATERIALS AND METHODS

2.1 | Participants

Data used for this study included two different cohorts. The first cohort included subjects enrolled in the Clinical Research Group 219 (KFO219) in Cologne. For the KFO cohort, rsfMRI and structural MRI data of 52 PD patients and 17 healthy controls were available. A subset of 41 PD patients and 13 healthy control subjects additionally underwent ^{18}F-DOPA-PET imaging. The average time difference between MRI and ^{18}F-DOPA-PET imaging was 29 days (SEM 8.05 days). All PD patients fulfilled the UK Brain Bank Criteria for PD (Gibb & Lees, 1988). All participants gave informed consent. The study was approved by the local ethics committee (EK12-265).

10970193, 2024, 10, Downloaded from https://onlinelibrary.wiley.com/doi/10.1002/hbm.26776 by Bibl. der Universitat zu Koln, Wiley Online Library on [13/11/2026]. See the Terms and Conditions (https://onlinelibrary.wiley.com/terms-and-conditions) on Wiley Online Library for rules of use; OA articles are governed by the applicable Creative Commons License

The second cohort was matched to the KFO cohort regarding age and sex and was composed of individuals registered in the PPMI. The PPMI dataset included 63 PD patients and 16 age- and sex-matched healthy controls. These subjects (1) had undergone a fixed rsfMRI protocol (see MRI acquisition), (2) were between 50 and 85 years old, and (3) had data of structural MRI, Unified Parkinson's Disease Rating Scale (UPDRS)-OFF, and DaT-SPECT imaging available. For PD individuals, the absolute time difference between the acquisition time points of these data and the rsfMRI acquisition date did not exceed 182 days. The PD group's average time difference between the DaT scan and rsfMRI acquisition was 12 days (SEM 2.29). For the control group, the difference was 728 days (SEM 165.22). All PD patients had a diagnosis of PD and exhibited bradykinesia and at least one of the following: resting tremor and/or rigidity.

Exclusion criteria for both cohorts included a history of other severe or neurological diseases and/or current medication that affects brain function, a clinical diagnosis of dementia, and MRI safety exclusion criteria. Any quality defects of the rsfMRI, like artifacts, phantoms, tilted planes, or cuts in the cortex, were excluded. The demographic characteristics of the two cohorts are summarized in Table 1.

2.2 | Clinical assessment

In both cohorts, disease severity in PD patients was assessed using the Movement Disorder Society UPDRS Part III (Goetz et al., 2008) in an unmedicated state (OFF). For the KFO dataset, this represented at least 12 h of withdrawal of dopamine replacement therapy or 72 h for extended release of dopamine agonists. In the PPMI cohort, 31 PD patients were taking medication. These subjects discontinued dopaminergic medication at least 6 h (16 h on average) before clinical examination (UPDRS-III). Furthermore, the Mini Mental State Examination (MMSE) in the KFO dataset and the Montreal Cognitive Assessment (MoCA) in the PPMI cohort were used as proxies for cognitive function. To establish comparability of these two tests, we converted the MoCA scores to MMSE scores according to a recently introduced table (Fasnacht et al., 2023).

2.3 | Assessment of dopamine loss

Measures of presynaptic dopamine deficiency were used to assess the possible impact of striatal dopamine availability on large-scale network connectivity dynamics. In the KFO cohort, ^{18}F-DOPA-PET imaging was used, which was acquired for a subset of 56 subjects on a 24-detector ring scanner (ECAT EXACT HRRT, Siemens) at the Max-Planck-Institute for Metabolism Research in Cologne. ^{18}F-DOPA-PET was performed in the morning after overnight fasting and OFF dopaminergic medication. The image processing procedure was previously described elsewhere (Hammes et al., 2019). Briefly, dopamine metabolism was assessed using a reference tissue model (Patlak plot) on dynamic scans comprising nine movement-corrected and spatially normalized frames. This data processing resulted in images exclusively representing the striatum's presynaptic dopamine synthesis capacity. Finally, the mean presynaptic dopamine synthesis capacity was extracted from four striatal volumes of interest (VOIs): the left and right putamen and caudate nucleus.

In the PPMI cohort, DaT-SPECT imaging was carried out in different imaging centers on different scanners. DaT-SPECT imaging was performed according to the PPMI standardized protocol to quantify DaTs in the striatum. Each imaging center reconstructed SPECT images using a standard iterative reconstruction algorithm and then corrected them for attenuation. Detailed imaging protocols can be comprehended here: https://www.ppmi-info.org/study-design/research-documents-and-sops. Our analysis used mean putamen and caudate values for both cohorts.

2.4 | MRI acquisition

An anatomical T1-weighted MRI and an rsfMRI series were acquired for each participant. In KFO, the structural T1-weighted images were obtained on a 3.0 T Siemens Magnetom Prisma scanner using multiband (SMS factor of 8) scanning combined with a 64 channel coil. The acquisition parameters were set as follows: repetition time (TR) = 2300 ms, echo time = 2.32 ms, flip angle = 8°, field of view =230 mm, slice thickness = 0.90 mm, voxel size = 0.9 × 0.9 × 0.9 mm, number of slices = 192. The rsfMRI series included a gradient echo-planar imaging sequence with interleaved acquisition mode using the following parameters: TR = 0.776 ms, echo time = 37.4 ms, flip angle = 55°, field view = 208 mm, voxel size = 2.0 × 2.0 × 2.0 mm, slice thickness = 2 mm. The acquisition time was 8 min and contained 617 time points comprised of 72 axial slices each.

In PPMI, the structural images were acquired on 3.0 T Siemens Magnetom scanners (Trio-A-Tim, Verio, or Prisma) using a slice thickness of 1 mm. The rsfMRI series used in the PPMI cohort was carried out in interleaved acquisition mode running the following protocol: TR = 2400 ms, echo time = 25.0 ms, voxel size = 3.3 × 3.3 × 3.3 mm, slice thickness 3.3 mm. The acquisition time was 8 min and 24 s, containing 210 time points composed of 40 axial slices each.

In both cohorts, subjects were asked to keep their eyes open and remain still.

2.5 | fMRI data preprocessing and motion control

Preprocessing was carried out using the CONN toolbox v20.b (Whitfield-Gabrieli & Nieto-Castanon, 2012) implemented in MATLAB (Matlab R2020b Update 4, MathWorks, Inc., Natick, Massachusetts, United States). A default preprocessing pipeline was used to normalize the images to the MNI (Montreal Neurological Institute) space (web.conn-toolbox.org/fmri-methods/preprocessing-pipeline). The pipeline includes spatial realignment, slice-timing correction, outlier identification, segmentation, normalization, and smoothing (Gaussian kernel 8 mm full-width half maximum).

Using the artifact removal tool included in CONN potential outlier scans caused by subject motion were identified, yielding six-

10970193, 2024, 10, Downloaded from https://onlinelibrary.wiley.com/doi/10.1002/hbm.26776 by Bibl. der Universitat zu Koln, Wiley Online Library on [13/11/2026]. See the Terms and Conditions (https://onlinelibrary.wiley.com/terms-and-conditions) on Wiley Online Library for rules of use; OA articles are governed by the applicable Creative Commons License

dimensional motion vectors composed of translational (x, y, z axes) and rotational (pitch, yaw, roll) displacement scores. These six displacement scores were each transformed into single framewise displacement (FD) values using a published formula (Power et al., 2012). Acquisitions were discarded if they showed a mean FD > ½ voxel size (1 mm in KFO and 1.65 mm in PPMI) and/or a maximum displacement of more than one voxel (2 mm in KFO and 3.3 mm in PPMI). According to these criteria, four PD patients and two healthy controls were excluded from the KFO cohort, resulting in a global mean FD of 0.19 mm for the final cohort. Finally, two PD patients and two healthy controls were excluded from the PPMI cohort, which resulted in an average FD of 0.34 mm.

2.6 | Identification of intrinsic connectivity networks

2.6.1 | Dimensionality reduction and group component definition

Independent group components were identified in a data-driven approach by means of data reduction and a spatial independent component analysis (ICA) utilizing the Group ICA fMRI toolbox (GIFT) (v3.0c, https://trendscenter.org/software/gift/). To obtain comparable components between the two cohorts, the group component identification was conducted in a pooled approach on all subjects of the two cohorts, involving healthy controls and PD patients (see Figure 2 left). The applied data reduction and ICA protocol followed previous dFC analyses (Allen et al., 2014; Damaraju et al., 2014; Díez-Cirarda et al., 2018; Fiorenzato et al., 2019; J. Kim et al., 2017): On the subject level, a principal component analysis (PCA) reduced the data to 120 principal components (PCs). At the group level, the concatenated reduced data was condensed to 100 PCs using the expectation maximization algorithm for PCA (Roweis, 1998). Following the data reduction step, a Infomax ICA algorithm (Himberg et al., 2004) decomposed the group-level data into independent networks (A. J. Bell & Sejnowski, 1995), producing a single set of 100 group independent components (ICs). Reliability through process stability was ensured by repeating the Infomax algorithm 20 times using the ICASSO method. Only components with a stability index >0.9 were selected, leaving 76 ICs for spatial characterization. Thereafter, a GICA-based back-reconstruction step was added to compute individual subject-specific spatial maps required for further analysis (Calhoun et al., 2001).

2.6.2 | Feature identification and thresholding

Of the 76 stable ICs, we identified 57 independent network components (INCs) utilizing identification criteria previously described (Allen et al., 2011; Allen et al., 2014): (1) peak activations located primarily in the gray matter, (2) low spatial overlap with known vascular and ventricular spaces, and (3) low susceptibility for artifacts. The resulting 57 INCs were subsequently grouped into 14 previously established resting-state networks (RSNs) (Allen et al., 2014; Shirer et al., 2012): Using the Dice similarity coefficient (a measure of spatial overlap), the INCs were sorted according to their highest spatial overlap with one of the RSNs. In seven instances, a single INC had a similar spatial overlap with several RSNs. For these cases, one of the RSN options was chosen by the shared decision of two experts (M.H., T.v.E.). An overview of the component patterns and corresponding RSNs can be found in Figure 1. With the preceding steps, including data reduction, ICA, feature identification, and back-reconstruction, we defined RSNs that share comparable activation patterns and anatomical locations across each individual and both cohorts. This approach enabled us to assess changes in RSN connectivity and compare these changes between individuals, groups, and cohorts.

2.7 | dFC analysis

The dFC analysis was conducted separately for each cohort. Using the temporal dFNC toolbox in GIFT, we combined two approaches: The sliding window approach, which determines changes in FC across time in single subjects, and the *k*-means clustering algorithm, which enables the extraction of reoccurring patterns of FC across time (see Figure 2 right).

2.7.1 | Sliding window approach

The sliding window approach was applied on time courses of the back-reconstructed subject-specific spatial maps obtained from the ICA, including both cohorts. Therefore, the same subject-specific maps were used in both analyses. These time courses were analyzed in frames of a defined length, called windows. The first window was set at the beginning of a time course and was then moved along the data by a predefined number of data points, defined as step variable. For each window, a covariance matrix was calculated, portraying the connectivity as covariance (correlation) between all INCs at that particular time. Each covariance matrix was composed of $(57 \times (57-1)/2 = 1596)$ features. Following previously established methods (Allen et al., 2014), a tapered window of 44 s (57 TRs in KFO and 18 TRs in PPMI) was used, which was convolved with a Gaussian kernel of 3 TR. The window was moved by 1TR steps along the 617 (KFO) and 210 (PPMI) TR scan, resulting in 493 (KFO) and 174 (PPMI) consecutive windows and their corresponding FC estimates (covariance matrices). Prior to further analysis, the FC estimates were Fisher Z transformed to improve the normality of Pearson's *r* distribution. To investigate the potential effect of TR, we matched the TRs of the two samples by down-sampling the KFOs TR to 2.328 ms (average of three scans with a TR of 0.776 ms). The results were comparable for manipulated and unmanipulated TR. Hence, the TRs for the current analysis were not altered.

10970193, 2024, 10, Downloaded from https://onlinelibrary.wiley.com/doi/10.1002/hbm.26776 by Bibl. der Universitat zu Koln, Wiley Online Library on [13/11/2026]. See the Terms and Conditions (https://onlinelibrary.wiley.com/terms-and-conditions) on Wiley Online Library for rules of use; OA articles are governed by the applicable Creative Commons License

2.7.2 | Clustering analysis

We applied the k-means clustering algorithm to all windowed FC estimates to assess reoccurring FC patterns. For each cohort, the clustering algorithm was initially performed on a defined subset of exemplary windows, chosen as the windows with local maxima in FC variance, and repeated 500 times on this set. The resulting centroids (cluster medians) were then used to initialize the clustering of all data on 69 subjects times 493 windows, equating to 35.496 instances in the case of KFO and 79 subjects times 174 windows, equating to 13,746 instances in the PPMI cohort. The similarity between each FC estimate and the cluster centers was determined using the L1 distance function (Aggarwal et al., 2001). The optimal number of clusters (k) was defined using the Elbow criterion, which independently yielded four valid clusters ($k = 4$) in both cohorts. Hence, based on the similarity of each FC matrix with the four obtained cluster centroids, all respective FC matrices were then categorized into one of the given four clusters (states). Reproducibility of the estimated states has previously been validated, showing that k-means clustering results yielded reproducible cluster centroids from both analyses with bootstrap resamples and split-half samples of subjects (Allen et al., 2014).

2.7.3 | Global state characteristics

To derive and compare the connectivity pattern associated with a state, connectivity matrices were calculated using in-house Python scripts (Asendorf, 2024; Damaraju et al., 2014): First, a subject median was computed for each state based on the subject windows assigned to that state. Second, subject medians for each state were used to derive median connectivity matrices for each state per cohort (see Figure 3). A state's connectivity strength was defined as the absolute sum of all correlation values in its median connectivity matrix. Notably, only correlation values higher or respectively lower than 10% of the highest and lowest correlation values were included to reduce the impact of noise on our measure. To define the proportionate similarity between two states, the Manhattan distance was calculated. According to the Manhattan distance, the most similar states were matched between cohorts. Next, to create state similarity profiles, we compared each individual tile (i.e., covariance of one INC with another) between the two matched states, respectively. For that purpose, we used Mann–Whitney U tests on all available subject medians for each tile (Asendorf, 2024; Damaraju et al., 2014). Hence, the comparison plots include the effect strength (r) of Mann–Whitney U tests for each tile. Only the effect strengths of results that were significant after FDR correction were reported. A state's occurrence was defined as the percentage of windows assigned to it. In an attempt to further characterize the connectivity pattern entailed in a state, we reported between-network correlations that stood out upon visual inspection.

2.7.4 | Calculation of temporal properties

Temporal properties of the dFC analysis were extracted, analyzed, and plotted for each cohort separately using in-house Python scripts (Asendorf, 2024): Based on the categorized data obtained by the clustering analysis in GIFT, state transition vectors were created, representing the assigned state for each window for each participant. To examine the temporal properties, we assessed four variables: average dwell time, total number of transitions, bidirectional transitions, and state attendance. The average dwell time was defined as the mean time spent in a particular state. We also assessed the total number of transitions between any states and the number of bidirectional transitions between specific pairs of states. A state was considered as attended if at least one window of that participant was assigned to that particular state.

2.8 | Statistical analyses

All statistical analyses were carried out using R (Rstudio ver. 2022.12.0) and Python (Spyder; Python ver. 3.10). Given that assumptions of normality and homoscedasticity were not met in terms of the dFC variables per cohort, nonparametric tests were applied. To minimize the influence of potential covariates, we corrected our statistical tests for age and sex. To this purpose, Whitney U tests were performed on the residuals of a linear model predicting the variable examined using age and sex. Further, Kendall's Tau correlations were corrected for age and sex using the ppcor package in R (S. Kim, 2015). Chi-squared tests cannot be corrected for covariates. However, all variables labeled as significantly different between groups by the Chi-squared test also showed a significant effect of group on the variable examined in a logistic regression model correcting for age and sex. Since PPMI is a multi-center cohort study, we sought to estimate the effect of inter-scanner variability on our results. Therefore, these tests were repeated with additional corrections for scanner identifiers. However, inter-scanner variability did not appear to affect our results. Thus, they were not reported in the results. Considering states with generally low attendance are a potential cause for unreliable statistics, we only included states attended by more than 50% of the cohort's subjects. Hence, state four (23%) of the KFO cohort and state two (23%) of the PPMI cohort were excluded from the statistical analyses. Corrections for multiple comparisons were carried out using the Dunn and Šidák criterion (Šidák, 1967).

2.8.1 | Group comparisons of dFC measures

Mann–Whitney U tests were performed to compare the PD and control groups in terms of variables derived from dFC analysis (i.e., average dwell time, fraction time, and number of transitions). For categorical variables like state attendance, Chi-squared tests were utilized.

10970193, 2024, 10, Downloaded from https://onlinelibrary.wiley.com/doi/10.1002/hbm.26776 by Bibl. der Universitat zu Koln, Wiley Online Library on [13/11/2026]. See the Terms and Conditions (https://onlinelibrary.wiley.com/terms-and-conditions) on Wiley Online Library for rules of use; OA articles are governed by the applicable Creative Commons License

2.8.2 | Correlation analyses—dFC Measures, dopamine loss, and behavior

To assess whether dFC measures were associated with cognitive test scores and motor performance, MMSE and UPDRS-III scores were correlated with average dwell time and the number of total and bidirectional transitions using two-sided rank correlation tests (Kendall's Tau). Besides, to examine whether temporal properties of a distinct state were associated with striatal dopamine signal, rank correlations were carried out between the mean synthesis capacity of the putamen and caudate VOIs and the dFC measurements.

3 | RESULTS

3.1 | Group characteristics

In both cohorts (see Table 1), we found no significant differences between the control group and the PD group in terms of sex, handedness, age and MMSE. In both cohorts, PD subjects had significantly fewer years of education and lower putaminal dopamine synthesis capacity or DaT availability, respectively.

Across cohorts, PD subjects did not show significant differences regarding sex, handedness, age, and UPDRS-III OFF scores. The PD group included in the KFO study had fewer years of education, lower MMSE scores, a higher L-dopa equivalent daily dose (LEDD), and a longer disease duration compared to the PD group of the PPMI cohort. Across cohorts, the KFO control group also showed lower values on the MMSE compared to PPMI controls. Sex, handedness, age, and education did not differ between the KFO control and the PPMI control group.

3.2 | Dynamic FC

3.2.1 | Global state characteristics

In both cohorts, we identified three distinct connectivity states that reoccurred in individuals throughout a resting-state scan and were present across subjects (see Figure 3).

For the KFO cohort, the two most frequently occurring states (a total of 64% of all windows) showed the most similar connectivity patterns (Manhattan distance of 119) across all state pairs (see Figure 3, top middle and top right panel). They mainly differed in overall connectivity strength. One state was clearly more interconnected with absolute correlation sums of 211.6 and 146.1, respectively. Hence, this state will be referred to as the more interconnected state, while the other state will be referred to as the lesser connected (LC) state of this state pair. Upon visual inspection, the pair can be characterized by strong correlations of the default mode network (DMN) with itself and parts of the left executive network and the language network. The other state occurred less frequently (a total of 22% of all windows) and exhibited high correlations for the ventral DMN with the visual networks, the language network and parts of the SMN, the auditory network, and the salience networks (see Figure 3 top left panel). As this state showed high interconnectivity for all RSN despite the auditory network, the dorsal DMN, and parts of the SMN, we will refer to this state as the globally integrated (GI) state.

Among all states of the PPMI cohort, two states exhibited the highest similarity measured by Manhattan distance (Manhattan distance of 107) (see Figure 3. bottom middle and bottom right). These states occurred by far the most (total of 73% of all windows) and primarily differed in connectivity strength (absolute correlation sum of 107.8 vs. 178.0). Hence, one state of the pair will be referred to as the more connected (MC) state, while the other will be termed the LC state. The other state occurred least often (a total of 16% of all windows) and showed a very distinctive connectivity pattern (see Figure 3 bottom left panel). On visual assessment, this state presented relatively high connectivity between the DMN, the primary visual, and the somatomotor networks. Following the framework in the KFO data, it will be referred to as the GI state.

The similarity between the sorted state profiles between both cohorts was described by Manhattan distance as follows: The highest similarity for the GI state and the LC state of the KFO cohort were the GI and the LC state of the PPMI cohort, respectively. For the MC state of the KFO, the LC state of the PPMI cohort was most similar. Further, upon visual inspection of the similarity matrices (see supplementary Figure 1), the LC states showed the highest similarity, while the MC and the GI states showed less similarity. A thorough visual assessment of the supplementary figure suggests that the indifferences between the MC and GI states were especially driven by the presence of negative correlations.

3.2.2 | Group differences in temporal properties

No significant group differences were found in terms of average dwell time in the KFO cohort and the PPMI cohort (see Figure 4a).

We determined the number of subjects having at least once dwelled in a state during acquisition, to compare state attendance between the groups. In the KFO cohort, no group differences were observed for state attendance. For the PPMI cohort, this yielded a higher state attendance of the GI state for the control group in contrast to the PD group ($X^2(1,\ N = 79) = 5.82,\ p = .016$) (see Figure 4b).

To determine further differences between groups, we compared the total number of transitions as well as the bidirectional transitions between pairs of states. For the KFO cohort, no group differences could be reported regarding total and bidirectional transitions. When assessing the distribution of the total number of transitions in the PPMI cohort, controls exhibited a higher number of transitions than PD patients in the ($U(N = 79) = 331,\ z = -2.10,\ p = .035$) (see Figure 4d). In terms of bidirectional transitions, controls showed a higher number of transitions between the GI and the MC state ($U(N = 79) = 276.5, z = -2.77, p = .006$) (see Figure 4c).

10970193, 2024, 10, Downloaded from https://onlinelibrary.wiley.com/doi/10.1002/hbm.26776 by Bibl. der Universitat zu Koln, Wiley Online Library on [13/11/2026]. See the Terms and Conditions (https://onlinelibrary.wiley.com/terms-and-conditions) on Wiley Online Library for rules of use; OA articles are governed by the applicable Creative Commons License

TABLE 1 Demographic and clinical data from both cohorts.

	PPMI				KFO				*p*-values			
	PD $n = 63$		Controls $n = 16$		PD $n = 52$		Controls $n = 17$		Controls vs. PD		PPMI vs. KFO	
	Mean (SD)/ Median (IQR)	Min-max	Mean (SD)/ Median (IQR)	Min-max	Mean (SD)/ Median (IQR)	Min-max	Mean (SD)/ Median (IQR)	Min-max	PPMI	KFO	PD	Controls
Sex (m/f)	38/25 m = 60%	-	13/3 m = 81%	-	35/17 m = 67%	-	9/8 m = 47%	-	$X^2(1, N = 79) = 1.61$, $p = .204$	$X^2(1, N = 69) = 1.46$, $p = .227$	$X^2(1, N = 115) = 0.95$, $p = .329$	$X^2(1, N = 33) = 3.77$, $p = .052$
Handedness (r/l/b)	59/3/1 r = 93%	-	14/1/1 r = 87%	-	42/3 r = 80%	-	15/1 r = 88%	-	$X^2(2, N = 79) = 1.2$, $p = .548$	$X^2(1, N = 61) = 0.0$, $p = 1.0$	$X^2(2, N = 108) = 0.94$, $p = .624$	$X^2(2, N = 32) = 0.91$, $p = .633$
Age	63.6 (7.9)	50.5–78.3	66.3 (7.4)	54.6–83.0	66.8 (8.0)	51–83	65.1 (7.1)	50–75	$U(N = 79) = 583.0$, $z = -0.70$, $p = .338$	$U(N = 69) = 393.5$, $z = -2.81$, $p = .503$	$U(N = 115) = 1292.0$, $z = -13.27$, $p = 0.052$	$U(N = 33) = 135.5$, $z = -4.92$, $p = 1.0$
Education (years)	15.0 (2.9)	8–23	17.0 (2.2)	13–22	13.4 (4.1)	0.0–20.0	16.6 (4.6)	0.0–21.0	$U(N = 79) = 722.0$, $z = 1.00$, $\mathbf{p = .006}$*	$U(N = 69) = 682.0$, $z = 1.21$, $\mathbf{p = .001}$*	$U(N = 115) = 2038.5$, $z = -9.08$, $\mathbf{p = .023}$*	$U(N = 33) = 115.0$, $z = -5.66$, $p = .452$
MMSE	30 (1)	24–30	30 (1)	28–30	29 (2)	24–30	29 (1)	27–30	$U(N = 79) = 592.5$, $z = -0.58$, $p = .191$	$U(N = 69) = 508.5$, $z = -1.21$, $p = .338$	$U(N = 115) = 2234.5$, $z = -7.98$, $\mathbf{p < .001}$*	$U(N = 33) = 199.5$, $z = -2.61$, $\mathbf{p = .011}$*
UPDRS-III OFF	23 (17)	7–51	-	-	25 (11.5)	8.0–56.0	-	-	-	-	$U(N = 115) = 1407.0$, $z = -12.63$, $p = .195$	-
Disease duration (years)	2.0 (1.3)	0.1–6.2	-	-	5.0 (3.5)	0.0–14.0	-	-	-	-	$U(N = 115) = 768.0$, $z = -16.22$, $\mathbf{p < .001}$*	-
DAT SPECT putamen	0.7 (0.31)	0.29–2.31	1.91 (0.3)	1.53–2.81	-	-	-	-	$U(N = 79) = 991.0$, $z = 4.28$, $\mathbf{p < .001}$*	-	-	-
^{18}F-DOPA-PET putamen	-	-	-	-	0.06 (0.02)	0.02–0.12	0.12 (0.01)	0.1–0.15	-	$U(N = 54) = 521.0$, $z = 3.31$, $\mathbf{p < .001}$*	-	-
LEDD	311.47 (416.35)	0–2200	-	-	468.52 (279.07)	50–1320	-	-	-	-	$U(N = 115) = 940.5$, $z = -15.25$, $\mathbf{p < .001}$*	-

Note: Deviation values are given in standard deviation (SD) and interquartile range (IQR) for ordinal values of UPDRS-III OFF and MMSE; MMSE = Mini Mental State Examination; UPDRS-III = Unified Parkinson's Disease Rating Scale-Part III, LEDD = L-dopa equivalent daily dose. *p*-values were obtained by a Mann–Whitney *U* test. The Chi-square test was used to test for differences in categorical variables like gender and handedness; *$p < .05$. Not for all subjects in the KFO cohort, handedness was available. Bold values are statistically significant.

10970193, 2024, 10, Downloaded from https://onlinelibrary.wiley.com/doi/10.1002/hbm.26776 by Bibl. der Universitat zu Koln, Wiley Online Library on [13/11/2026]. See the Terms and Conditions (https://onlinelibrary.wiley.com/terms-and-conditions) on Wiley Online Library for rules of use; OA articles are governed by the applicable Creative Commons License

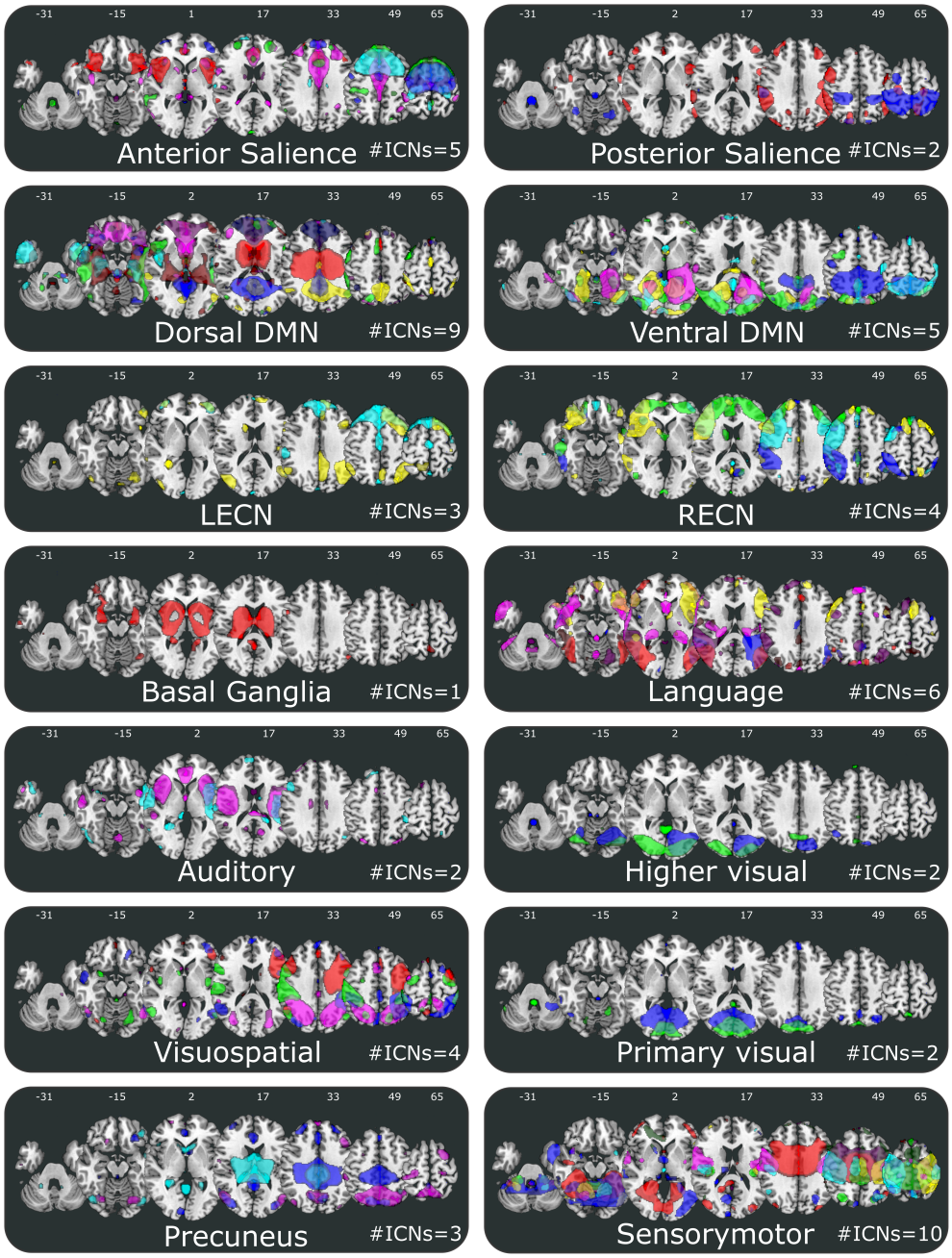

FIGURE 1 Composite maps of the 57 independent network components (INCs) identified by group independent component analysis (ICA). Based on their anatomical and functional properties, 57 INCs were grouped into the 14 resting-state networks (RSNs) for FC previously established by Shirer et al., 2012. Each color in the composite maps corresponds to a single INC. The number of ICNs sorted into each RSN is stated in the bottom right corner of each panel. DMN, default mode network; LECN, left executive network; RECN, right executive network.

3.2.3 | Correlation between striatal dopamine availability, dFC measures, and clinical measures

dFC with clinical measures

We tested for an association between MMSE and UPDRS-III scores with the number of bidirectional transitions, average dwell times, and total number of transitions. In the KFO cohort, an association between UPDRS-III scores and the number of bidirectional transitions between the GI and the LC state ($\tau_b(N = 52) = -.245$; $p = .012$) was observed in the PD group. For the MMSE scores, no associations with dFC were found in the KFO cohort. In the PPMI cohort, a correlation analysis revealed significant negative associations between UPDRS-III motor scores and average time spent in the GI state ($\tau_b(N = 63) = -.276$, $p = .002$) and the MC state ($\tau_b(N = 63) = -.201$, $p = .022$). Moreover, we found negative associations of the UPDRS-III and the total number of transitions ($\tau_b(N = 63) = -.307$, $p < .001$) and number of bidirectional transitions between the GI and the LC state ($\tau_b(N = 63) = -.227$, $p = .010$) and the MC and the LC state ($\tau_b(N = 63) = -.213$, $p = .015$) in the PD group. In the PPMI cohort, no associations of dFC variables with MMSE were found.

Dopamine with clinical measures

In a subsequent step, we tested whether dopaminergic insufficiency of the two striatal VOIs was associated with either cognitive scores or

10970193, 2024, 10, Downloaded from https://onlinelibrary.wiley.com/doi/10.1002/hbm.26776 by Bibl. der Universitat zu Koln, Wiley Online Library on [13/11/2026]. See the Terms and Conditions (https://onlinelibrary.wiley.com/terms-and-conditions) on Wiley Online Library for rules of use; OA articles are governed by the applicable Creative Commons License

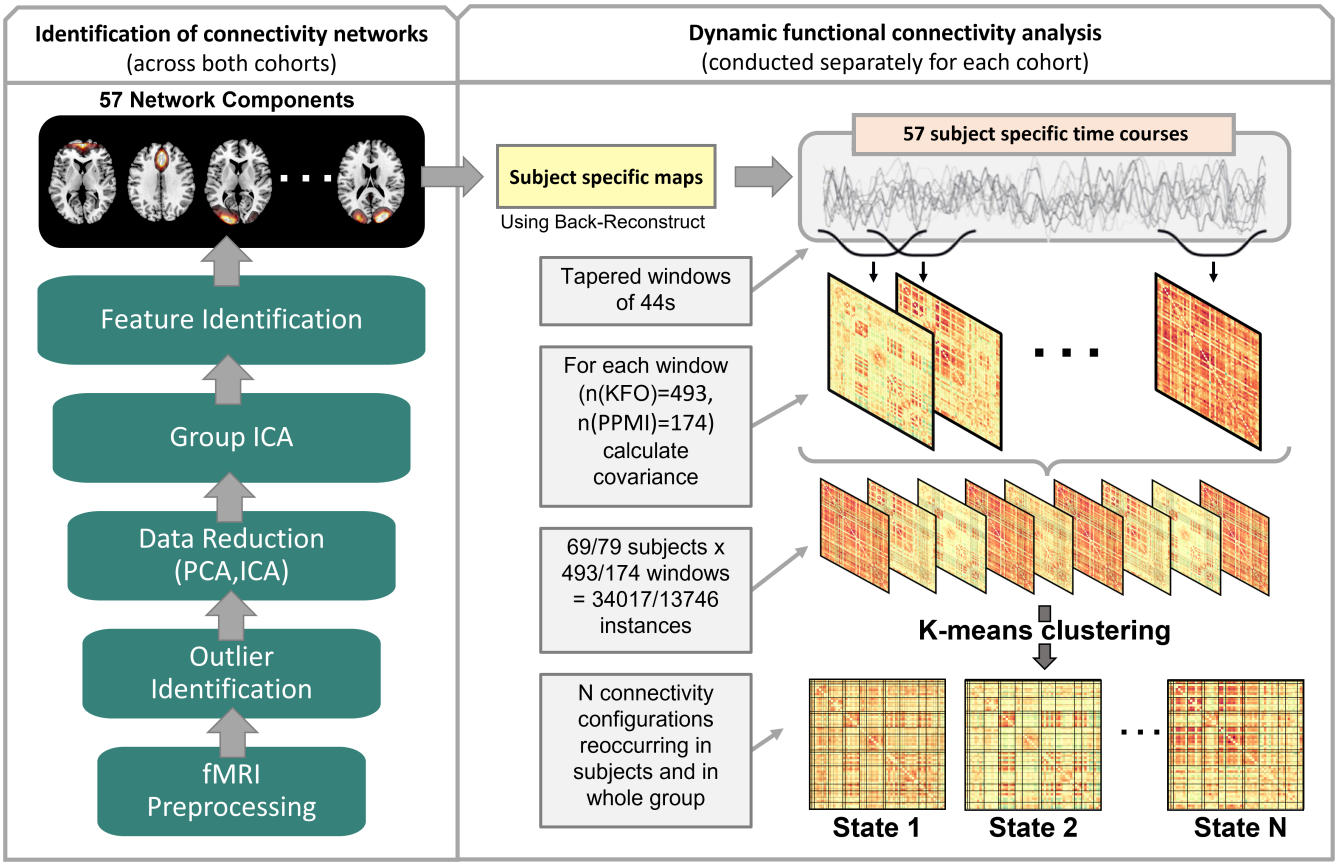

FIGURE 2 Schematic of the dynamic functional connectivity analysis pipeline: The green boxes represent the general steps to retrieve independent network components (INCs) from both cohorts. Afterward, a back reconstruction step resulted in subject-specific spatial maps and time courses for each INC. Via the sliding window approach utilizing tapered windows of 44 s length, correlation matrices were obtained for each patient across the entire scan for each cohort. With the k-means clustering algorithm, the correlation matrices of the entire cohort were clustered according to similarity.

motor function in the PD groups. The correlation analysis yielded a significant negative correlation between the mean putamen values and UPDRS-III OFF scores in the KFO cohort (τ_b ($N = 41$) $= -.226$, $p = .043$) and the PPMI cohort (τ_b ($N = 63$) $= -.180$, $p = .040$). Both results did not withstand correction for multiple comparisons ($k = 2$: adj. $p = .025$). In both cohorts, we did not find an association between cognitive scores of the MMSE and mean dopamine scores in the putamen or the caudate.

Dopamine with dFC

As the average dwell time, the number of bidirectional transitions, and the number of total transitions correlated with UPDRS-III off scores in the PPMI cohort, we tested the association between striatal dopamine availability and the three dFC properties across the PD group in both cohorts. Inside the KFO PD group, no such associations between dFC variables and dopamine synthesis capacity could be reported. Inside the PPMI cohort, average time spent in the GI state correlated with the mean DaT availability in the putamen ($\tau_b(N = 63) = .22$, $p = .012$) and the caudate ($\tau_b(N = 63) = .216$, $p = .014$). The number of total transitions was also associated with mean DAT availability in the putamen ($\tau_b(N = 63) = .341$, $p < .001$) and the caudate ($\tau_b(N = 63) = .24$, $p = .006$). In terms of bidirectional transitions we observed an association of the number of transitions between the GI and MC state with mean DAT availability in the caudate ($\tau_b(N = 63) = .225$, $p = .010$) and the LC and MC with the DAT availability in the putamen ($\tau_b(N = 63) = .225$, $p = .021$). We further found an association of bidirectional transitions between the GI and MC ($\tau_b(N = 63) = .183$, $p = .038$) state and GI the LC ($\tau_b(N = 63) = .182$, $p = .038$) with the mean DAT availability in the putamen. These associations, however, did not survive correction for multiple comparisons ($k = 2$: adj. $p = .025$).

4 | DISCUSSION

The primary aim of this study was to elucidate dopamine's association with whole-brain network dynamics in PD. This study used two matched cohorts to assess the reproducibility of the dFC results. Ultimately, we found PD-specific network dynamics in the PPMI cohort: A decrease in the number of transitions and a lower overall presence

10970193, 2024, 10, Downloaded from https://onlinelibrary.wiley.com/doi/10.1002/hbm.26776 by Bibl. der Universitat zu Koln, Wiley Online Library on [13/11/2026]. See the Terms and Conditions (https://onlinelibrary.wiley.com/terms-and-conditions) on Wiley Online Library for rules of use; OA articles are governed by the applicable Creative Commons License

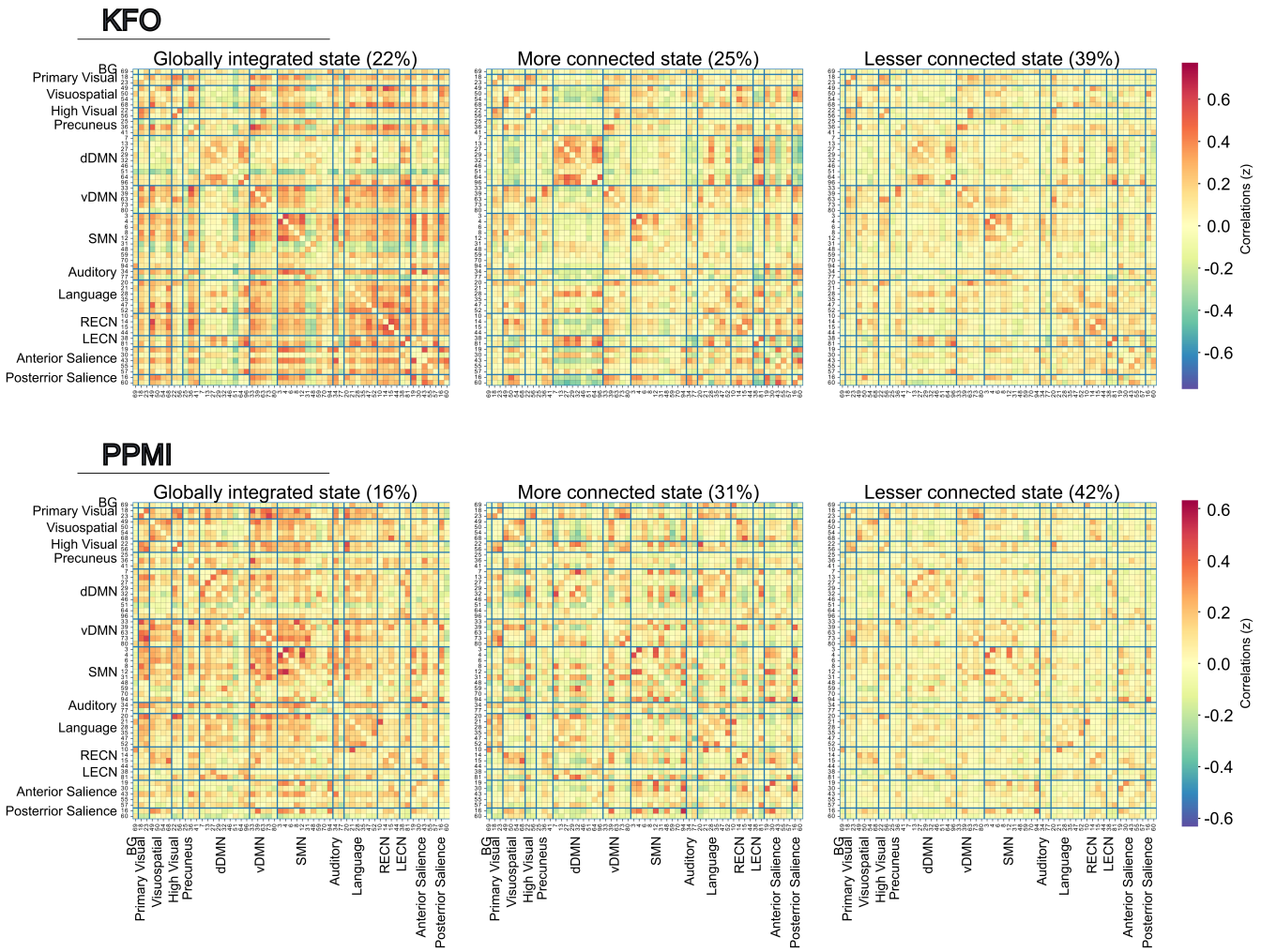

FIGURE 3 Dynamic functional connectivity (FC) states along the whole sample ($k = 3$) for each cohort. Each cluster is summarized in one FC map portraying FC within and between resting-state networks (RSNs) (portioned by thick blue lines) in pairwise correlations. The correlations were Fisher z transformed and averaged across all subjects, then inverse z-transformed for display. The total percentage of windows assigned to the state is shown. The value of correlations is represented in the color bar; the red color represents positive and blue negative correlations. The diagonal represents the correlations of the subnetwork by itself and is thereby one.

of the GI state. Since these specific features of dFC were negatively associated with UPDRS-III scores (one also in KFO), we suspect a high transition frequency toward a GI state and an increased presence of a GI state to facilitate motor performance. As these have further been shown to be associated with striatal dopamine availability, dopamine appears to play an essential role in mediating those large-scale network dynamics in early PD patients. Notably, our results were not stable across cohorts, suggesting that the dFC alterations depended on cohort composition.

Employing dFC on two cohorts, we identified three connectivity states in both cohorts that followed the same pattern. In both cohorts, there were two states of high total occurrence, showing the highest similarity regarding connectivity patterns of all three states: One was highly connected, while the other was less connected. The last state, less frequent in both cohorts, was characterized by a more global, integrated connectivity pattern. Hence, using two independent k-means clustering approaches, we disentangled two similar connectivity cluster profiles for both cohorts, enabling us to compare inside group differences between cohorts. In the PPMI cohort, we found the overall expression of these states and the dynamic transition between states to be group-dependent. For the KFO cohort, however, we did not observe any differences between groups. Hence, if not explicitly stated, all the findings discussed below were found only inside the PPMI cohort.

First, PD individuals of the PPMI cohort showed overall decreased transitions between states. Indeed, most of the previous studies in whole-brain dFC in PD reported differences in the total number of transitions (Cordes et al., 2018; Díez-Cirarda et al., 2018; Fiorenzato et al., 2019). However, their results are conflicting. While one study reported a higher number of transitions in PD (Díez-Cirarda et al., 2018), two other studies showed a lower transitioning frequency in PD patients compared to controls (Cordes et al., 2018; Fiorenzato et al., 2019). Interestingly, in two of these studies, this trend solely depended on cognitive status (Díez-Cirarda et al., 2018;

10970193, 2024, 10, Downloaded from https://onlinelibrary.wiley.com/doi/10.1002/hbm.26776 by Bibl. der Universitat zu Koln, Wiley Online Library on [13/11/2026]. See the Terms and Conditions (https://onlinelibrary.wiley.com/terms-and-conditions) on Wiley Online Library for rules of use; OA articles are governed by the applicable Creative Commons License

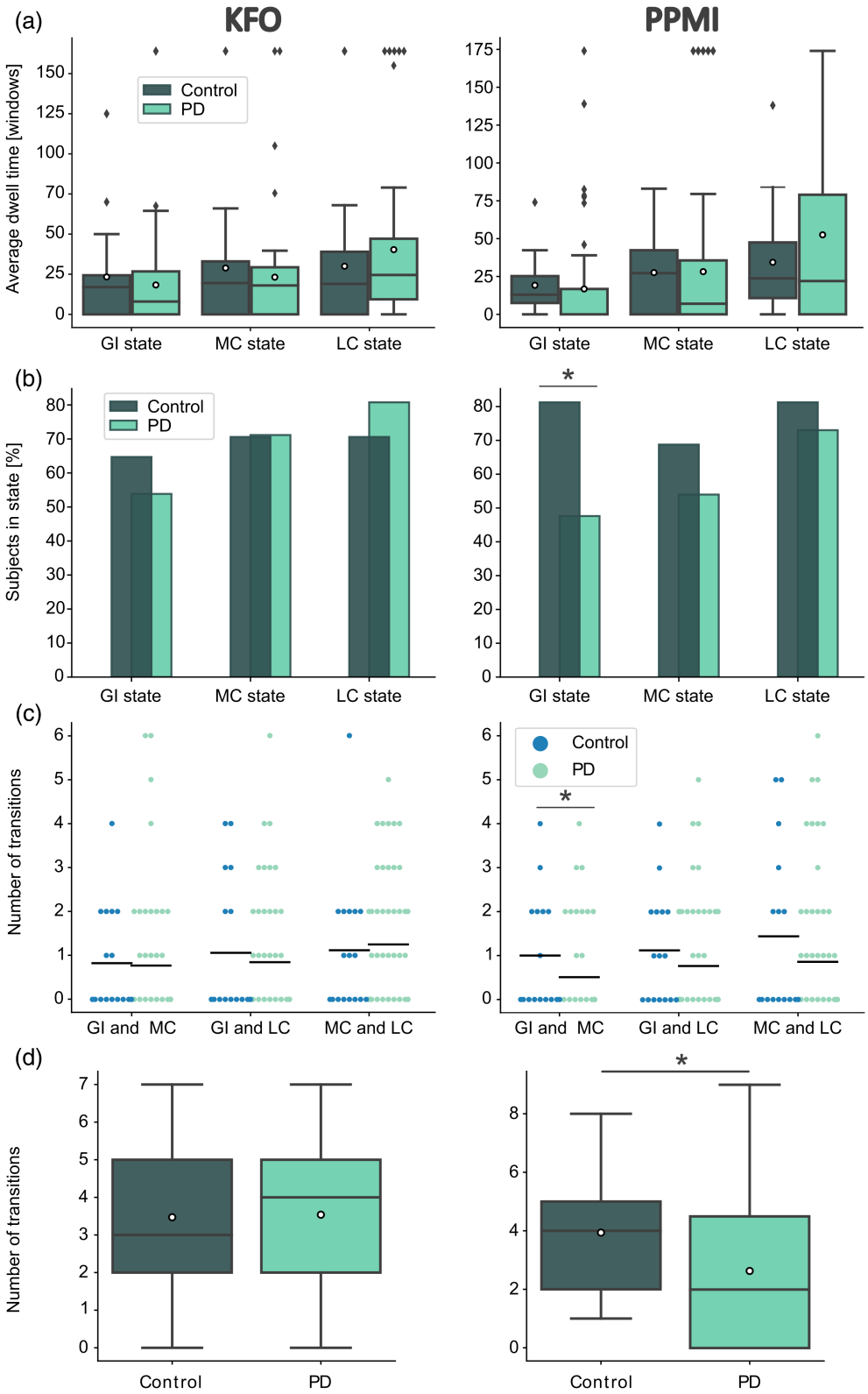

FIGURE 4 Temporal properties of dynamic functional connectivity (dFC) states for Parkinson's disease and healthy control groups. (a) Boxplot portraying the distribution of the average time spent in the globally integrated (GI), the more connected (MC), and the lesser connected (LC) state for each cohort. Each colored box represents the interquartile range (IQR), with the median plotted as a thin line and the mean represented by a white dot. The whiskers specify minimum and maximum. Outliers are shown in the form of diamonds. Time is specified in windows. (b) Percentual proportion of subjects having dwelled in the GI, the MC, and the LC state at least once during a scan. A Chi-squared test tested for between-group differences. (c) Group-specific number of transitions between the pairs of states GI and MC, GI and LC, and MC and LC. The black lines indicate the mean values. Within-group differences were tested via the Friedmann test. (d) Boxplot portraying the distribution of the total number of transitions between all states. Mann–Whitney *U* tests tested for between-group differences; $^{*}p < .05$.

Fiorenzato et al., 2019). Although our findings suggest that PD patients exhibit limited dynamics in dwelling behavior, these results were not associated with deteriorating cognitive abilities, as reported by Fiorenzato et al. (2019), or overall decreased cognitive flexibility, as suggested by Nomi et al. (2017). Against this body of studies, we found features of dFC in the PPMI and the KFO cohort to be associated with motor performance: In PPMI, PD patients who, in total, transitioned less between states showed higher motor impairments

10970193, 2024, 10, Downloaded from https://onlinelibrary.wiley.com/doi/10.1002/hbm.26776 by Bibl. der Universitat zu Koln, Wiley Online Library on [13/11/2026]. See the Terms and Conditions (https://onlinelibrary.wiley.com/terms-and-conditions) on Wiley Online Library for rules of use; OA articles are governed by the applicable Creative Commons License

according to the UPDRS-III. This result contradicts previous observations linking better motor performance with reduced transition behavior (J. Kim et al., 2017).

Moreover, we observed the same relationship when comparing the specific transitioning patterns between groups. PD patients who specifically transitioned more often between the GI and the LC state showed better motor performance in both cohorts. In contrast, most of the studies mentioned above identified only two states in their study or did not investigate differences in transitioning patterns if more states were present. Hence, across two separate cohorts, we are the first to report associations of specific transitioning patterns with motor performance in PD. These associations suggest that overall high network dynamics and dynamics between particular connectivity configurations are relevant in motor control. Thus, in PD, the underlying mechanisms facilitating these dynamic transitions between states of global integration and segregation seem to be impaired. Intriguingly, our results in PPMI further imply that this ability to generally transition between states and to specifically transition between globally segregated and integrated states depends on the integrity of the striatal dopaminergic system. This notion is based on two findings. First, we observed, trend significant, the well-known relationship between the decline in DaT signal and the increase in the UPDRS-III motor score (Benamer et al., 2000; Pirker, 2003; Seibyl et al., 1995) inside the PPMI PD group and the KFO cohort. Second, in PPMI PD patients, the ability to dynamically transition between all states, and the ability to transition specifically between the GI and LC state, were associated with caudal and putaminal DaT availability.

Further, fewer PD patients of the PPMI group visited the globally integrated state at least once during an 8-min acquisition compared to controls. Hence, many PD individuals missed spending time in a state characterized by high interconnectivity between networks. Together with our previous results indicating that dynamic transitions between states of global integration and segregation are impaired in PD, these results extend the notion that PD patients may have problems transitioning specifically into a state of global integration. Interestingly, another study longitudinally investigating dFC changes in PPMI data revealed a decrease in dwell time in a state similar to the GI state and an increase in dwell time for a state corresponding to the LC state (Cao et al., 2023). Their results suggest that hypocoupling worsens in the course of PD (Cao et al., 2023). We did not find a decrease in average dwell time in the GI state for PD. Yet, our other findings in the same cohort suggest this worsening of hypocoupling to be caused by an inability to transition into a state with high interconnectivity. Central to this, in our study, the average time spent in the GI state in the PPMI cohort and the number of bidirectional transitions between the GI and the LC state in both cohorts were positively associated with motor performance. This suggests the increased presence of hypocoupling and decreased dynamics between integrated and segregated connectivity configurations to be related to poor motor output. Similar associations were reported in whole-brain dFC before; however, again, the opposite effect was reported (Kim et al., 2017).

Nevertheless, another recent study showed levodopa intake to increase the dwell time in a state with the strongest functional coupling between the fronto-parietal network (FPN) and the SMN (Chen et al., 2021). OFF medication, this mean dwell time was reduced again in the same PD patients (Chen et al., 2021). Notably, this dopamine-associated change in mean dwell time was negatively associated with UPDRS-III scores, highlighting that altered dFC features are associated with motor performance and, particularly related to dopamine. In our PPMI cohort, we could reproduce these findings with a direct measure of dopaminergic impairment, as the mean dwell time in the globally integrated state was positively associated with the mean DaT signal in the putamen and the caudate. While Chen and colleagues' study was focused on dynamics between the SMN and networks involved in top-down motor control, our study assessed network dynamics on a whole-brain level. Hence, our results obtained in the PPMI cohort extend their view of SMN and FPN stability to be dopamine-dependent, pointing to the fact that global integration of the SMN with other non-motor associated networks is dopamine dependent and relevant to sustaining proper motor output.

According to our results in both cohorts, we suspect that in early PD patients, network changes are affiliated with motor function. In particular, the overall presence of globally interconnected states and high dynamics toward a state of high interconnectivity seem to facilitate motor performance. As in PPMI, these have further been shown to be related to striatal dopamine availability, dopamine appears to play an essential role in mediating those large-scale network dynamics in early PD patients. With these findings, we provide a novel mechanism for how dopamine might modulate motor control in PD and highlight the potential of investigating large-scale network dynamics in a disease context. In particular, investigating bidirectional transitions between connectivity states, which have never been assessed in PD, provided novel insights into how dopamine might contribute to motor functions.

Importantly, although the state profiles of both cohorts were very well matched, we did not observe any group differences in the KFO cohort. In this section, we will discuss potential reasons for that. First, we will assess how demographical differences and cohort composition might have fueled differences in dFC results across cohorts. Second, we will investigate whether the methodological approach itself might be the underlying cause of the varying results in both cohorts.

Comparing the demographics of both PD groups revealed two things: First, the PD individuals of the KFO cohort were more advanced in the progression of the disease than the ones of the PPMI cohort. Accordingly, KFO PD patients presented a longer disease duration and a higher LEDD. In the course of the disease, the brain undergoes a functional reorganization of the RSNs, which may even occur before the onset of clinical symptoms (Tessitore et al., 2019). Accordingly, also PD-specific dFC alterations were shown to increase over time (Cao et al., 2023). Since the PD individuals of the KFO cohort showed a more advanced disease progression, we would expect these changes to be more profoundly expressed in the dFC metrics of the KFO PD group cohort compared to the PPMI PD group. However, contrary to our expectations, the KFO cohort did not show any group differences in dFC metrics to the healthy control group.

10970193, 2024, 10, Downloaded from https://onlinelibrary.wiley.com/doi/10.1002/hbm.26776 by Bibl. der Universitat zu Koln, Wiley Online Library on [13/11/2026]. See the Terms and Conditions (https://onlinelibrary.wiley.com/terms-and-conditions) on Wiley Online Library for rules of use; OA articles are governed by the applicable Creative Commons License

Second, KFO PD individuals showed lower levels of education and lower scores in cognitive tests despite inherently difficult comparisons between countries. In healthy subjects, cognitive performance (Cabral et al., 2017) and flexibility (Nomi et al., 2017) have been associated with the ability to switch dynamically between states. Further, also PD-specific alterations of dFC have been associated with increased cognitive impairment (Boon et al., 2020; Díez-Cirarda et al., 2018; Fiorenzato et al., 2019). Hence, contrary to the obtained results, we would expect the KFO cohort to be even more likely to show between-group differences than PPMI. This expectation is further supported by findings involving education, cognition, and FC in healthy aging. Age- and education-related changes in FC were associated with memory performance (Montemurro et al., 2023). Moreover, a cohort of healthy controls and multiple sclerosis with longer education showed higher dynamics and better cognitive performances (Lin et al., 2018).

In summary, we could not identify any demographical feature that, in accordance with the current literature, explains why we obtained such imbalanced results between both cohorts. However, we assume that other unrecognized and untracked demographical differences might drive dFC results. Assessing the cohort composition in more detail may lead to a clearer verdict as to why the group differences obtained in the PPMI cohort were not observed in the KFO cohort. Unfortunately, no more detailed and comparable cohort features were available.

Next, we will address how the methodological approach might have impacted the results. One could argue that due to the unconstrained nature of resting-state experiments, the concept of rsfMRI itself may appear challenging when reproducing results in two cohorts. Nonetheless, static RSNs were proven to have high levels of reproducibility across imaging sessions (Biswal et al., 2010; Shehzad et al., 2009) and different subjects (Damoiseaux et al., 2006; Shehzad-et al., 2009). Through our data-driven approach that included both cohorts simultaneously, we established RSNs that were similarly expressed across all individuals of both cohorts. This enabled us to compare differences between groups inside the cohort and the obtained results across cohorts. By choosing comparatively similar sample sizes for controls and PD patients in both cohorts, we ensured that individuals of one particular cohort did not dominate the RSN composition. However, the clinical presentation of PD is heterogeneous. Previous reports indicate a difference in DMN and striatal connectivity in PD patients with tremor-predominant and primarily akinetic rigid symptoms (Karunanayaka et al., 2016; Zhang et al., 2015). Based on this, although PD groups were matched across cohorts, RSN connectivity might have varied in both PD groups due to different subtype ratios.

Furthermore, inside the cohorts, group sizes deviated highly from each other. Controls comprised 25.4% of the PPMI and 32.7% of the KFO cohort. Hence, overall RSN architecture could have been driven by PD RSN composition. Despite that argument, during our definition of meaningful components, the RSNs identified by the ICA considerably overlapped with RSNs previously established in groups of younger healthy controls (Shirer et al., 2012). Refining RSNs for each group in each cohort separately would resolve these two issues. However, they would critically dampen the between-group and especially the between-cohort comparability of our dFC results.

Likewise, the dFC approach might be susceptible to technical differences in data acquisition. Hence, although the same analysis pipelines were used, alterations in data acquisition may interfere differently with dFC results. The most notable alteration in data acquisition is the inter-scanner variability. In contrast to the KFO study, where all subjects were scanned on the same scanner, PPMI, as a multicenter study, includes individuals who were scanned on various scanners and scanner types. Importantly, to test the influence of inter-scanner variability on our results we additionally corrected our results in PPMI for scanner identifiers. The obtained results did not differ from our original results. Hence, we are confident that the variations among scanners in the PPMI dataset have a negligible effect on our findings. Further, it has been suggested that the duration of a dFC-appropriate resting-state acquisition should be at least 10 min (Hindriks et al., 2016). Hence, the extended acquisition time in the PPMI resting-state protocol of 8.5 min might have been better suited to a dFC approach than the KFO's 8-min acquisitions. Moreover, the cohort's acquisition paradigms varied drastically in TR. Hence, the analysis was carried out for the KFO cohort separately, once with a TR adjusted to the PPMI dataset and once with an unadjusted TR. Although these two approaches equally did not produce any sign group differences regarding dFC variables for the KFO cohort, we cannot rule out that the different TRs might affect dFC results. Nevertheless, as changing the KFO's TR by downsampling would entail a significant manipulation of the input data, we kept the data as they were. Interestingly, a preceding study provided evidence of the reproducibility of basic connectivity patterns amidst inter-regional connections over 7500 scans composing "probably" mixed independent resting-state datasets of healthy and diseased individuals (Abrol et al., 2017). However, all these scans followed the same acquisition protocol, and only eight of these scans deviated in TR from the other scans. Vital to mention at this point is a recent study investigating the relationship of dFC alterations with non-motor symptoms of PD in a PPMI cohort. This study used the same analysis pipeline with slightly altered settings (50s windows, Yeo atlas). Intriguingly, this study found astonishingly similar state patterns to those we achieved for the PPMI cohort in our approach (Cao et al., 2023). This demonstrates the reproducibility of state patterns across different analysis parameters and cohort composition in one of our cohorts. Further, this high similarity in sorted state patterns signifies that joining both cohorts in one ICA did not alter the state pattern composition of our PPMI cohort.

Considering all this, we can summarize that we identified differences in cohort composition and acquisition parameters that could have caused variation in the between-group differences observed in both cohorts. Yet, we did not identify one specific feature in methodology or cohort composition that we consider highly influential. We suspect these differences in the results to be driven by differences in

10970193, 2024, 10, Downloaded from https://onlinelibrary.wiley.com/doi/10.1002/hbm.26776 by Bibl. der Universitat zu Koln, Wiley Online Library on [13/11/2026]. See the Terms and Conditions (https://onlinelibrary.wiley.com/terms-and-conditions) on Wiley Online Library for rules of use; OA articles are governed by the applicable Creative Commons License

cohort composition that were not assessed within the framework of this study, like disease subtype ratio or lifestyle factors. This again underlines the need for deep phenotyping in neuroimaging datasets, as a more detailed description of the cohorts and more significant group sizes would have been highly relevant to performing an effective group matching.

5 | CONCLUSION

Our findings in the PPMI cohort illustrate that PD patients exhibit altered network dynamics compared to healthy controls. These alterations are defined by a lower prevalence for integrated connectivity states and decreased transition frequency between a globally integrated and a LC state. With these findings, we supply a potential mechanism for how dopaminergic neurodegeneration drives global changes in connectivity underlying motor dysfunction in PD. However, most of these results were obtained for only one of two cohorts. Therefore, it will be valuable to reassess these findings and their replicability in two bigger, effectively matched cohorts. Furthermore, it will be interesting to investigate whether the reported impairment of network dynamics is already observable in prodromal stages of PD, such as in patients with REM-sleep behavioral disorder.

AUTHOR CONTRIBUTIONS

AA, MH, and TVE were responsible for the design and conduct of the analysis. AA wrote the first draft of the manuscript, which co-authors carefully reviewed.

ACKNOWLEDGMENT

The authors are grateful for the patience and commitment of every participant participating in the study.

CONFLICT OF INTEREST STATEMENT

AA reports no conflicts of interest. MH reports receiving research funding from the German Research Foundation (DFG). T. van Eimeren received honoraria, stipends or speaker fees from the Lundbeck Foundation, Gain Therapeutics, Orion Pharma, Lundbeck Pharma, Atheneum, and the International Movement Disorders Society. He receives materials from Life Molecular Imaging and Lilly Pharma. He owns stocks of the corporations NVIDIA, Microsoft and I.B.M. GRF serves as an editorial board member of Cortex, Neurological Research and Practice, NeuroImage: Clinical, Zeitschrift für Neuropsychologie, DGNeurologie, and Info Neurologie & Psychiatrie; receives royalties from the publication of the books Funktionelle MRT in Psychiatrie und Neurologie, Neurologische Differentialdiagnose, and SOP Neurologie; receives royalties from the publication of the neuropsychological tests KAS and Köpps; received honoraria for speaking engagements from Deutsche Gesellschaft für Neurologie (DGN) and Forum für medizinische Fortbildung FomF GmbH. HT was supported by the Cologne Clinician Scientist Program (CCSP) / Faculty of Medicine / University of Cologne. Funded by the Deutsche Forschungsgemeinschaft (DFG, German Research Foundation) (Project No. 431549029, 413543196)

DATA AVAILABILITY STATEMENT

The data that support the findings of this study are available from the corresponding author upon reasonable request.

ORCID

Thilo van Eimeren https://orcid.org/0000-0002-6951-2325

REFERENCES

Abrol, A., Damaraju, E., Miller, R. L., Stephen, J. M., Claus, E. D., Mayer, A. R., & Calhoun, V. D. (2017). Replicability of time-varying connectivity patterns in large resting state fMRI samples. *NeuroImage*, *163*, 160–176. https://doi.org/10.1016/J.NEUROIMAGE.2017.09.020

Aggarwal, C. C., Hinneburg, A., & Keim, D. A. (2001). On the surprising behavior of distance metrics in high dimensional space. In J. Van den Bussche & V. Vianu (Eds.), *Database theory—ICDT 2001* (pp. 420–434). Springer-Verlag. https://doi.org/10.1007/3-540-44503-x_27

Allen, E. A., Damaraju, E., Plis, S. M., Erhardt, E. B., Eichele, T., & Calhoun, V. D. (2014). Tracking whole-brain connectivity dynamics in the resting state. *Cerebral Cortex*, *24*(3), 663–676. https://doi.org/10.1093/cercor/bhs352

Allen, E. A., Erhardt, E. B., Damaraju, E., Gruner, W., Segall, J. M., Silva, R. F., Havlicek, M., Rachakonda, S., Fries, J., Kalyanam, R., Michael, A. M., Caprihan, A., Turner, J. A., Eichele, T., Adelsheim, S., Bryan, A. D., Bustillo, J., Clark, V. P., Ewing, S. W. F., … Calhoun, V. D. (2011). A baseline for the multivariate comparison of resting-state networks. *Frontiers in Systems Neuroscience*, *5*(FEBRUARY 2011), 1–23. https://doi.org/10.3389/fnsys.2011.00002

Asenbaum, S., Brücke, T., Pirker, W., Podreka, I., Angelberger, P., Wenger, S., Wöber, C., Müller, C., & Deecke, L. (1997). Imaging of dopamine transporters with Iodine-123- and SPECT in Parkinson's disease. *Society of Nuclear Medicine*, *38*(1), 1–6. https://jnm.snmjournals.org/content/38/1/1

Asendorf, A. L. (2024). *Handling-GIFT* (Vol. 1). GitHub. Retrieved from https://github.com/Asendorfa/Handling-GIFT/tree/main

Bell, A. J., & Sejnowski, T. J. (1995). An information-maximization approach to blind separation and blind deconvolution. *Neural Computation*, *7*(6), 1129–1159. https://doi.org/10.1162/neco.1995.7.6.1129

Bell, P. T., Gilat, M., O'Callaghan, C., Copland, D. A., Frank, M. J., Lewis, S. J. G., & Shine, J. M. (2015). Dopaminergic basis for impairments in functional connectivity across subdivisions of the striatum in Parkinson's disease. *Human Brain Mapping*, *36*(4), 1278–1291. https://doi.org/10.1002/hbm.22701

Benamer, H. T. S., Patterson, J., Wyper, D. J., Hadley, D. M., Macphee, G. J. A., & Grosset, D. G. (2000). Correlation of Parkinson's disease severity and duration with 123 I-FP-CIT SPECT striatal uptake. *Movement Disorders*, *15*(4), 692–698. https://doi.org/10.1002/1531-8257

Biswal, B. B., Mennes, M., Zuo, X. N., Gohel, S., Kelly, C., Smith, S. M., Beckmann, C. F., Adelstein, J. S., Buckner, R. L., Colcombe, S., Dogonowski, A. M., Ernst, M., Fair, D., Hampson, M., Hoptman, M. J., Hyde, J. S., Kiviniemi, V. J., Kötter, R., Li, S. J., … Milham, M. P. (2010). Toward discovery science of human brain function. *Proceedings of the National Academy of Sciences of the United States of America*, *107*(10), 4734–4739. https://doi.org/10.1073/pnas.0911855107

Boon, L. I., Hepp, D. H., Douw, L., van Geenen, N., Broeders, T. A. A., Geurts, J. J. G., Berendse, H. W., & Schoonheim, M. M. (2020). Functional connectivity between resting-state networks reflects decline in

10970193, 2024, 10, Downloaded from https://onlinelibrary.wiley.com/doi/10.1002/hbm.26776 by Bibl. der Universitat zu Koln, Wiley Online Library on [13/11/2026]. See the Terms and Conditions (https://onlinelibrary.wiley.com/terms-and-conditions) on Wiley Online Library for rules of use; OA articles are governed by the applicable Creative Commons License

executive function in Parkinson's disease: A longitudinal fMRI study. *NeuroImage: Clinical*, *28*, 102468. https://doi.org/10.1016/J.NICL.2020.102468

Cabral, J., Vidaurre, D., Marques, P., Magalhães, R., Silva Moreira, P., Miguel Soares, J., Deco, G., Sousa, N., & Kringelbach, M. L. (2017). Cognitive performance in healthy older adults relates to spontaneous switching between states of functional connectivity during rest. *Scientific Reports*, *7*(1), 1–13. https://doi.org/10.1038/s41598-017-05425-7

Calhoun, V. D., Adali, T., Pearlson, G. D., & Pekar, J. J. (2001). Spatial and temporal independent component analysis of functional MRI data containing a pair of task-related waveforms. *Human Brain Mapping*, *13*(1), 43–53. https://doi.org/10.1002/hbm.1024

Calhoun, V. D., Miller, R., Pearlson, G., & Adali, T. (2014). The chronnectome: Time-varying connectivity networks as the next frontier in fMRI data discovery. *Neuron*, *84*(2), 262–274. https://doi.org/10.1016/J.NEURON.2014.10.015

Cao, Y., Si, Q., Tong, R., Zhang, X., Li, C., & Mao, S. (2023). Abnormal dynamic functional connectivity changes correlated with non-motor symptoms of Parkinson's disease. *Frontiers in Neuroscience*, *17*, 1116111. https://doi.org/10.3389/FNINS.2023.1116111/BIBTEX

Chang, C., & Glover, G. (2010). Time-frequency dynamics of resting-state brain connectivity measured with fMRI. *NeuroImage*, *50*(1), 81–98. https://doi.org/10.1016/j.neuroimage.2009.12.011.Time-frequency

Chen, L., Bedard, P., Hallett, M., & Horovitz, S. G. (2021). Dynamics of top-down control and motor networks in Parkinson's disease. *Movement Disorders*, *36*(4), 916–926. https://doi.org/10.1002/MDS.28461

Cole, D. M., Oei, N. Y. L., Soeter, R. P., Both, S., Van Gerven, J. M. A., Rombouts, S. A. R. B., & Beckmann, C. F. (2013). Dopamine-dependent architecture of cortico-subcortical network connectivity. *Cerebral Cortex*, *23*(7), 1509–1516. https://doi.org/10.1093/cercor/bhs136

Cools, R. (2011). Dopaminergic control of the striatum for high-level cognition. *Current Opinion in Neurobiology*, *21*(3), 402–407. https://doi.org/10.1016/j.conb.2011.04.002

Cordes, D., Zhuang, X., Kaleem, M., Sreenivasan, K., Yang, Z., Mishra, V., Banks, S. J., Bluett, B., & Cummings, J. L. (2018). Advances in functional magnetic resonance imaging data analysis methods using empirical mode decomposition to investigate temporal changes in early Parkinson's disease. *Alzheimer's and Dementia*, *4*, 372–386. https://doi.org/10.1016/j.trci.2018.04.009

Costa, A., Peppe, A., Mazzù, I., Longarzo, M., Caltagirone, C., & Carlesimo, G. A. (2014). Dopamine treatment and cognitive functioning in individuals with Parkinson's disease: The "cognitive flexibility" hypothesis seems to work. *Behavioural Neurology*, *2014*, 1–11. https://doi.org/10.1155/2014/260896

Córdova-Palomera, A., Kaufmann, T., Persson, K., Alnæs, D., Doan, N. T., Moberget, T., Lund, M. J., Barca, M. L., Engvig, A., Brækhus, A., Engedal, K., Andreassen, O. A., Selbæk, G., & Westlye, L. T. (2017). Disrupted global metastability and static and dynamic brain connectivity across individuals in the Alzheimer's disease continuum. *Scientific Reports*, *7*(1), 1–14. https://doi.org/10.1038/srep40268

Damaraju, E., Allen, E. A., Belger, A., Ford, J. M., McEwen, S., Mathalon, D. H., Mueller, B. A., Pearlson, G. D., Potkin, S. G., Preda, A., Turner, J. A., Vaidya, J. G., Van Erp, T. G., & Calhoun, V. D. (2014). Dynamic functional connectivity analysis reveals transient states of dysconnectivity in schizophrenia. *NeuroImage: Clinical*, *5*(July), 298–308. https://doi.org/10.1016/j.nicl.2014.07.003

Damoiseaux, J. S., Rombouts, S. A. R. B., Barkhof, F., Scheltens, P., Stam, C. J., Smith, S. M., & Beckmann, C. F. (2006). Consistent resting-state networks across healthy subjects. *Proceedings of the National Academy of Sciences of the United States of America*, *103*(37), 13848–13853. https://doi.org/10.1073/pnas.0601417103

de Lacy, N., Doherty, D., King, B. H., Rachakonda, S., & Calhoun, V. D. (2017). Disruption to control network function correlates with altered dynamic connectivity in the wider autism spectrum. *NeuroImage: Clinical*, *15*, 513–524. https://doi.org/10.1016/J.NICL.2017.05.024

Díez-Cirarda, M., Strafella, A. P., Kim, J., Peña, J., Ojeda, N., Cabrera-Zubizarreta, A., & Ibarretxe-Bilbao, N. (2018). Dynamic functional connectivity in Parkinson's disease patients with mild cognitive impairment and normal cognition. *NeuroImage: Clinical*, *17*(July 2017), 847–855. https://doi.org/10.1016/j.nicl.2017.12.013

Fasnacht, J. S., Wueest, A. S., Berres, M., Thomann, A. E., Krumm, S., Gutbrod, K., Steiner, L. A., Goettel, N., & Monsch, A. U. (2023). Conversion between the Montreal Cognitive Assessment and the Mini-Mental Status Examination. *Journal of the American Geriatrics Society*, *71*(3), 869–879. https://doi.org/10.1111/JGS.18124

Fiorenzato, E., Strafella, A. P., Kim, J., Schifano, R., Weis, L., Antonini, A., & Biundo, R. (2019). Dynamic functional connectivity changes associated with dementia in Parkinson's disease. *Brain*, *142*(9), 2860–2872. https://doi.org/10.1093/brain/awz192

Fu, Z., Tu, Y., Di, X., Du, Y., Pearlson, G. D., Turner, J. A., Biswal, B. B., Zhang, Z., & Calhoun, V. D. (2018). Characterizing dynamic amplitude of low-frequency fluctuation and its relationship with dynamic functional connectivity: An application to schizophrenia. *NeuroImage*, *180*, 619–631. https://doi.org/10.1016/J.NEUROIMAGE.2017.09.035

Gibb, W. R. G., & Lees, A. J. (1988). The relevance of the Lewy body to the pathogenesis of idiopathic Parkinson's disease. *Journal of Neurology, Neurosurgery, and Psychiatry*, *51*, 745–752. https://doi.org/10.1136/jnnp.51.6.745

Goetz, C. G., Tilley, B. C., Shaftman, S. R., Stebbins, G. T., Fahn, S., Martinez-Martin, P., Poewe, W., Sampaio, C., Stern, M. B., Dodel, R., Dubois, B., Holloway, R., Jankovic, J., Kulisevsky, J., Lang, A. E., Lees, A., Leurgans, S., LeWitt, P. A., Nyenhuis, D., … Zweig, R. M. (2008). Movement Disorder Society-sponsored revision of the Unified Parkinson's Disease Rating Scale (MDS-UPDRS): Scale presentation and clinimetric testing results. *Movement Disorders*, *23*(15), 2129–2170. https://doi.org/10.1002/MDS.22340

Hammes, J., Theis, H., Giehl, K., Hoenig, M. C., Greuel, A., Tittgemeyer, M., Timmermann, L., Fink, G. R., Drzezga, A., Eggers, C., & Van Eimeren, T. (2019). Dopamine metabolism of the nucleus accumbens and fronto-striatal connectivity modulate impulse control. *Brain*, *142*(3), 733–743. https://doi.org/10.1093/brain/awz007

Himberg, J., Hyvärinen, A., & Esposito, F. (2004). Validating the independent components of neuroimaging time series via clustering and visualization. *NeuroImage*, *22*(3), 1214–1222. https://doi.org/10.1016/j.neuroimage.2004.03.027

Hindriks, R., Adhikari, M. H., Murayama, Y., Ganzetti, M., Mantini, D., Logothetis, N. K., & Deco, G. (2016). Can sliding-window correlations reveal dynamic functional connectivity in resting-state fMRI? *NeuroImage*, *127*, 242–256. https://doi.org/10.1016/j.neuroimage.2015.11.055

Hutchison, M., Womelsdorf, T., Allen, E., Bandettini, P., Valhoun, V., Penna, S., Duyn, J., Glover, G., Gonzalez-Castillo, J., Handwerker, D., Keilholz, S., Kiviniemi, V., & Leopold, D. (2013). Dynamic functional connectivity: Promise, issues, and interpretations. *NeuroImage*, *80*, 1–43. https://doi.org/10.1016/j.neuroimage.2013.05.079

Jin, C., Jia, H., Lanka, P., Rangaprakash, D., Li, L., Liu, T., Hu, X., & Deshpande, G. (2017). Dynamic brain connectivity is a better predictor of PTSD than static connectivity. *Human Brain Mapping*, *38*(9), 4479–4496. https://doi.org/10.1002/HBM.23676

Jones, D. T., Vemuri, P., Murphy, M. C., Gunter, J. L., Senjem, M. L., Machulda, M. M., Przybelski, S. A., Gregg, B. E., Kantarci, K., Knopman, D. S., Boeve, B. F., Petersen, R. C., & Jack, C. R. (2012). Non-stationarity in the "resting brain's" modular architecture. *PLoS One*, *7*(6), e39731. https://doi.org/10.1371/journal.pone.0039731

Kaiser, R. H., Whitfield-Gabrieli, S., Dillon, D. G., Goer, F., Beltzer, M., Minkel, J., Smoski, M., Dichter, G., & Pizzagalli, D. A. (2015). Dynamic resting-state functional connectivity in major depression.

10970193, 2024, 10, Downloaded from https://onlinelibrary.wiley.com/doi/10.1002/hbm.26776 by Bibl. der Universitat zu Koln, Wiley Online Library on [13/11/2026]. See the Terms and Conditions (https://onlinelibrary.wiley.com/terms-and-conditions) on Wiley Online Library for rules of use; OA articles are governed by the applicable Creative Commons License

Neuropsychopharmacology, *41*(7), 1822–1830. https://doi.org/10.1038/npp.2015.352

Karunanayaka, P. R., Lee, E. Y., Lewis, M. M., Sen, S., Eslinger, P. J., Yang, Q. X., & Huang, X. (2016). Default mode network differences between rigidity- and tremor-predominant Parkinson's disease. *Cortex*, *81*, 239–250. https://doi.org/10.1016/J.CORTEX.2016.04.021

Kim, J., Criaud, M., Cho, S. S., Díez-Cirarda, M., Mihaescu, A., Coakeley, S., Ghadery, C., Valli, M., Jacobs, M. F., Houle, S., & Strafella, A. P. (2017). Abnormal intrinsic brain functional network dynamics in Parkinson's disease. *Brain*, *140*(11), 2955–2967. https://doi.org/10.1093/brain/awx233

Kim, S. (2015). Ppcor: An R package for a fast calculation to semi-partial correlation coefficients. *Communications for Statistical Applications and Methods*, *22*(6), 665–674. https://doi.org/10.5351/CSAM.2015.22.6.665

Li, W., Lao-Kaim, N. P., Roussakis, A. A., Martín-Bastida, A., Valle-Guzman, N., Paul, G., Soreq, E., Daws, R. E., Foltynie, T., Barker, R. A., Hampshire, A., & Piccini, P. (2020). Longitudinal functional connectivity changes related to dopaminergic decline in Parkinson's disease. *NeuroImage: Clinical*, *28*(August), 102409. https://doi.org/10.1016/j.nicl.2020.102409

Lin, S. J., Vavasour, I., Kosaka, B., Li, D. K. B., Traboulsee, A., MacKay, A., & McKeown, M. J. (2018). Education, and the balance between dynamic and stationary functional connectivity jointly support executive functions in relapsing–remitting multiple sclerosis. *Human Brain Mapping*, *39*(12), 5039–5049. https://doi.org/10.1002/HBM.24343

Liu, F., Wang, Y., Li, M., Wang, W., Li, R., Zhang, Z., Lu, G., & Chen, H. (2017). Dynamic functional network connectivity in idiopathic generalized epilepsy with generalized tonic–clonic seizure. *Human Brain Mapping*, *38*(2), 957–973. https://doi.org/10.1002/hbm.23430

Liégeois, R., Li, J., Kong, R., Orban, C., Van De Ville, D., Ge, T., Sabuncu, M. R., & Yeo, B. T. T. (2019). Resting brain dynamics at different timescales capture distinct aspects of human behavior. *Nature Communications*, *10*(1), 1–9. https://doi.org/10.1038/s41467-019-10317-7

Lurie, D. J., Kessler, D., Bassett, D. S., Betzel, R. F., Breakspear, M., Keilholz, S., Kucyi, A., Liégeois, R., Lindquist, M. A., McIntosh, A. R., Poldrack, R. A., Shine, J. M., Thompson, W. H., Bielczyk, N. Z., Douw, L., Kraft, D., Miller, R. L., Muthuraman, M., Pasquini, L., … Calhoun, V. D. (2020). Questions and controversies in the study of time-varying functional connectivity in resting fMRI. *Network Neuroscience*, *4*(1), 30–69. https://doi.org/10.1162/NETN_A_00116

Montemurro, S., Filippini, N., Ferrazzi, G., Mantini, D., Arcara, G., & Marino, M. (2023). Education differentiates cognitive performance and resting state fMRI connectivity in healthy aging. *Frontiers in Aging Neuroscience*, *15*, 1168576. https://doi.org/10.3389/fnagi.2023.1168576

Nomi, J. S., Vij, S. G., Dajani, D. R., Steimke, R., Damaraju, E., Rachakonda, S., Calhoun, V. D., & Uddin, L. Q. (2017). Chronnectomic patterns and neural flexibility underlie executive function. *NeuroImage*, *147*(3), 861–871. https://doi.org/10.1016/j.neuroimage.2016.10.026

Pirker, W. (2003). Correlation of dopamine transporter imaging with parkinsonian motor handicap: How close is it? *Movement Disorders*, *18*(S7), S43–S51. https://doi.org/10.1002/MDS.10579

Power, J. D., Barnes, K. A., Snyder, A. Z., Schlaggar, B. L., & Petersen, S. E. (2012). Spurious but systematic correlations in functional connectivity MRI networks arise from subject motion. *NeuroImage*, *59*(3), 2142–2154. https://doi.org/10.1016/j.neuroimage.2011.10.018

Rashid, B., Arbabshirani, M. R., Damaraju, E., Cetin, M. S., Miller, R., Pearlson, G. D., & Calhoun, V. D. (2016). Classification of schizophrenia and bipolar patients using static and dynamic resting-state fMRI brain connectivity. *NeuroImage*, *134*, 645–657. https://doi.org/10.1016/J.NEUROIMAGE.2016.04.051

Rieckmann, A., Gomperts, S. N., Johnson, K. A., Growdon, J. H., & Van Dijk, K. R. A. (2015). Putamen-midbrain functional connectivity is related to striatal dopamine transporter availability in patients with Lewy body diseases. *NeuroImage: Clinical*, *8*, 554–559. https://doi.org/10.1016/j.nicl.2015.06.001

Rolinski, M., Griffanti, L., Piccini, P., Roussakis, A. A., Szewczyk-Krolikowski, K., Menke, R. A., Quinnell, T., Zaiwalla, Z., Klein, J. C., Mackay, C. E., & Hu, M. T. M. (2016). Basal ganglia dysfunction in idiopathic REM sleep behaviour disorder parallels that in early Parkinson's disease. *Brain*, *139*(8), 2224–2234. https://doi.org/10.1093/BRAIN/AWW124

Roweis, S. (1998). EM algorithms for PCA and SPCA. In Advances in NIPS '97: Proceedings of the 1997 Conference on Advances in Neural Information Processing Systems 10 (pp. 626–632). Retrieved from https://papers.nips.cc/paper_files/paper/1997/hash/d9731321ef4e063ebbee79298fa36f56-Abstract.html

Ruppert, M. C., Greuel, A., Tahmasian, M., Schwartz, F., Stürmer, S., Maier, F., Hammes, J., Tittgemeyer, M., Timmermann, L., van Eimeren, T., Drzezga, A., & Eggers, C. (2020). Network degeneration in Parkinson's disease: Multimodal imaging of nigro-striato-cortical dysfunction. *Brain*, *143*(3), 944–959. https://doi.org/10.1093/brain/awaa019

Sakoğlu, Ü., Pearlson, G. D., Kiehl, K. A., Wang, Y. M., Michael, A. M., & Calhoun, V. D. (2010). A method for evaluating dynamic functional network connectivity and task-modulation: Application to schizophrenia. *Magnetic Resonance Materials in Physics, Biology and Medicine*, *23*(5–6), 351–366. https://doi.org/10.1007/s10334-010-0197-8

Schumacher, J., Peraza, L. R., Firbank, M., Thomas, A. J., Kaiser, M., Gallagher, P., O'Brien, J. T., Blamire, A. M., & Taylor, J. P. (2019). Dynamic functional connectivity changes in dementia with Lewy bodies and Alzheimer's disease. *NeuroImage: Clinical*, *22*, 101812. https://doi.org/10.1016/J.NICL.2019.101812

Seibyl, J. P., Marchek, K. L., Quinlan, D., Sheff, K., Zoghbi, S., Zea-Ponce, Y., Baldwin, R. M., Fussell, B., Smith, E. O., Charney, D. S., Hoffer, P. B., & Innis, R. B. (1995). Decreased single-photon emission computed tomographic [123I]β-CIT striatal uptake correlates with symptom severity in Parkinson's disease. *Annals of Neurology*, *38*(4), 589–598. https://doi.org/10.1002/ANA.410380407

Šidák, Z. (1967). Rectangular confidence regions for the means of multivariate normal distributions. *Journal of the American Statistical Association*, *62*(318), 626–633. https://doi.org/10.1080/01621459.1967.10482935

Shehzad, Z., Kelly, A. M. C., Reiss, P. T., Gee, D. G., Gotimer, K., Uddin, L. Q., Lee, S. H., Margulies, D. S., Roy, A. K., Biswal, B. B., Petkova, E., Castellanos, F. X., & Milham, M. P. (2009). The resting brain: Unconstrained yet reliable. *Cerebral Cortex*, *19*(10), 2209–2229. https://doi.org/10.1093/CERCOR/BHN256

Shirer, W. R., Ryali, S., Rykhlevskaia, E., Menon, V., & Greicius, M. D. (2012). Decoding subject-driven cognitive states with whole-brain connectivity patterns. *Cerebral Cortex*, *22*(1), 158–165. https://doi.org/10.1093/cercor/bhr099

Tessitore, A., Cirillo, M., & De Micco, R. (2019). Functional connectivity signatures of Parkinson's disease. *Journal of Parkinson's Disease*, *9*(4), 637–652. https://doi.org/10.3233/JPD-191592

Tozlu, C., Jamison, K., Gauthier, S. A., & Kuceyeski, A. (2021). Dynamic functional connectivity better predicts disability than structural and static functional connectivity in people with multiple sclerosis. *Frontiers in Neuroscience*, *15*, 763966. https://doi.org/10.3389/fnins.2021.763966

Vidaurre, D., Llera, A., Smith, S. M., & Woolrich, M. W. (2021). Behavioural relevance of spontaneous, transient brain network interactions in fMRI. *NeuroImage*, *229*, 117713. https://doi.org/10.1016/J.NEUROIMAGE.2020.117713

Whitfield-Gabrieli, S., & Nieto-Castanon, A. (2012). Conn: A functional connectivity toolbox for correlated and anticorrelated brain networks. *Brain Connectivity*, *2*(3), 125–141. https://doi.org/10.1089/brain.2012.0073

Wu, T., Long, X., Zang, Y., Wang, L., Hallett, M., Li, K., & Chan, P. (2009). Regional homogeneity changes in patients with Parkinson's disease.

10970193, 2024, 10, Downloaded from https://onlinelibrary.wiley.com/doi/10.1002/hbm.26776 by Bibl. der Universitat zu Koln, Wiley Online Library on [13/11/2026]. See the Terms and Conditions (https://onlinelibrary.wiley.com/terms-and-conditions) on Wiley Online Library for rules of use; OA articles are governed by the applicable Creative Commons License

Human Brain Mapping, *30*(5), 1502–1510. https://doi.org/10.1002/hbm.20622

Yue, J. L., Li, P., Shi, L., Lin, X., Sun, H. Q., & Lu, L. (2018). Enhanced temporal variability of amygdala-frontal functional connectivity in patients with schizophrenia. *NeuroImage: Clinical*, *18*, 527–532. https://doi.org/10.1016/J.NICL.2018.02.025

Zhang, J., Wei, L., Hu, X., Xie, B., Zhang, Y., Wu, G. R., & Wang, J. (2015). Akinetic-rigid and tremor-dominant Parkinson's disease patients show different patterns of intrinsic brain activity. *Parkinsonism & Related Disorders*, *21*(1), 23–30. https://doi.org/10.1016/j.parkreldis.2014.10.017

Zhi, D., Calhoun, V. D., Lv, L., Ma, X., Ke, Q., Fu, Z., Du, Y., Yang, Y., Yang, X., Pan, M., Qi, S., Jiang, R., Yu, Q., & Sui, J. (2018). Aberrant dynamic functional network connectivity and graph properties in major depressive disorder. *Frontiers in Psychiatry*, *9*, 371911. https://doi.org/10.3389/fpsyt.2018.00339

SUPPORTING INFORMATION

Additional supporting information can be found online in the Supporting Information section at the end of this article.

How to cite this article: Asendorf, A. L., Theis, H., Tittgemeyer, M., Timmermann, L., Fink, G. R., Drzezga, A., Eggers, C., Ruppert-Junck, M. C., Pedrosa, D. J., Hoenig, M. C., & van Eimeren, T. (2024). Dynamic properties in functional connectivity changes and striatal dopamine deficiency in Parkinson's disease. *Human Brain Mapping*, *45*(10), e26776. https://doi.org/10.1002/hbm.26776

10970193, 2024, 10, Downloaded from https://onlinelibrary.wiley.com/doi/10.1002/hbm.26776 by Bibl. der Universitat zu Koln, Wiley Online Library on [13/11/2026]. See the Terms and Conditions (https://onlinelibrary.wiley.com/terms-and-conditions) on Wiley Online Library for rules of use; OA articles are governed by the applicable Creative Commons License